nature communications

Article

https://doi.org/10.1038/s41467-025-63632-7

The pathogen effector BcSSP2 suppresses the NPC phase separation to facilitate *Botrytis cinerea* infection

Received: 18 May 2023

Accepted: 26 August 2025

Published online: 29 September 2025

Check for updates

Jiaojiao Wang[1,2,7] ✉, Dewei Wu[2,3,7], Gaofeng Pei[4,7], Yupei Wang[2,7], Xiaokang Liu[2], Shiping Tian[5,6], Zhanquan Zhang[5,6], Xiaolin Zhang[2], Pilong Li[4] ✉, Daoxin Xie[2] ✉ & Xiaoyi Shan[2] ✉

Biomolecular phase separation-mediated immunity was recently uncovered as an important strategy of plants and animals for their survival in the challenging environment. Effectors are powerful weapons evolved by pathogens to overcome host defense response for effective infection. However, plant pathogen effectors were rarely identified to suppress the phase separation-mediated host defense response. Here, we report a pathogen effector that disrupts phase separation process in host cells to suppress host defense response and facilitate pathogen infection. We identify a host-internalized effector protein BcSSP2 from a disastrous pathogen *Botrytis cinerea* targets the central barrier of plant nuclear pore complex (NPC). BcSSP2 disrupts the phase separation of NUP62 and attenuates phase separation-dependent nuclear transport of immune regulator MPK3 to suppress plant defense response for effective pathogen infection. Intriguingly, BcSSP2 homologs are widely distributed among necrotrophic ascomycetes and also interfere with NUP62 phase separation, suggesting that disrupting plant NPC phase separation might be an evolutionarily conserved strategy evolved by these necrotrophic pathogens to facilitate their infection.

Plants and animals have developed effective immune systems to protect them from a variety of aggressive pathogens for their survival in nature[1]. These host immune systems were regulated by a multitude of mechanisms including RNAi-based immunity[2], resistance gene-regulated immunity[3] and autophagy-triggered immunity[4]. Phase separation, a driving force for the formation of various membraneless organelles, deeply involves in the health maintenance of mammals[5–7], including the innate immune signaling activated by the viral DNA-induced phase separation of cGAS[8–10], and severe neurodegenerative diseases caused by abnormal phase separation of FUS, tau and TDP-43[11]. In plants, phase separation of plant nuclear pore complex (NPC) was uncovered to regulate diverse plant defense responses against fungal and bacterial infection and insect attack[12], phase separation of NPR1, GBPL1/3, HEM1 and Toll/interleukin-1 receptor were found to regulate plant resistance to bacterial infection[13–16]. These results suggest that phase separation-mediated defense response has emerged as a general mechanism to regulate plant defense against diverse biotic stresses.

[1]College of Biological Sciences and Biotechnology, Beijing Forestry University, Beijing, China. [2]MOE Key Laboratory of Bioinformatics, Tsinghua University-Peking University Joint Center for Life Sciences, and School of Life Sciences, Tsinghua University, Beijing, China. [3]China-Uruguay Joint Laboratory on Soybean Research and Innovation, Institute of Crop Sciences, Chinese Academy of Agricultural Sciences, Beijing, China. [4]State Key Laboratory of Membrane Biology, Frontier Research Center for Biological Structure, School of Life Sciences, Tsinghua University; Tsinghua University-Peking University Joint Center for Life Sciences, Beijing, China. [5]Institute of Botany, Chinese Academy of Sciences, Beijing, China. [6]University of Chinese Academy of Sciences, Beijing, China. [7]These authors contributed equally: Jiaojiao Wang, Dewei Wu, Gaofeng Pei, Yupei Wang ✉e-mail: nxywjj@163.com; pilongli@tsinghua.edu.cn; daoxinlab@mail.tsinghua.edu.cn; shanxy80@tsinghua.edu.cn

To achieve successful infection, pathogens also have evolved sophisticated mechanisms to fight against host defense response. Secreting effector proteins is a powerful strategy to counter host immune system, which is commonly adopted by almost all types of pathogens including bacteria, fungi and viruses[17–20]. Enormous efforts made by biologists worldwide have uncovered a huge amount of pathogen effectors that suppress host defense response via different mechanisms, including targeting host immune regulators to affect their transcription, translation or posttranslational modifications[21–24], disturbing cellular organelles[25], and binding with host small RNAs[26]. However, effectors from plant pathogens have rarely been shown to suppress the phase separation-mediated host defense response.

In this study, we reported the effector protein BcSSP2 from *Botrytis cinerea* (*B. cinerea*), one of the most disastrous plant pathogens causing severe economic losses worldwide[27,28], is secreted into plant cells to target the central barrier of plant NPC, interfere with phase separation of host NPC central barrier, and consequently suppress the phase separation-dependent nuclear transport of a key immune regulator MPK3, leading to attenuated plant defense response and thus facilitating pathogen infection.

Results

BcSSP2 is a putative effector from *B. cinerea*

B. cinerea is generally regarded as a necrotrophic pathogen which usually secrets lytic enzymes, oxalic acid and phytotoxins to extracellular spaces of host cells for infection[27,28]. It is so far unknown whether *B. cinerea* delivers effector proteins into plant cells to disturb host immunity for successful infection. We collected *B. cinerea* hyphae from the in vitro culture or the infected *Arabidopsis* leaves to compare the hyphal transcriptomic profiles. Among the genes upregulated in *B. cinerea* infection process (Supplementary Data 1, 2), 15 genes were shortlisted as effector candidates due to the typical effector features of other well-studied pathogens such as RXLR motif and cysteine-rich region in their encoding proteins (Fig. 1a; Supplementary Data 3)[29].

Recent studies revealed that suppression of host immunity in biotrophic stage is required for necrotrophic pathogens to establish colonization[30,31]. As shown in Supplementary Fig. 1, *B. cinerea* takes a considerable period to establish colonization and rot plant tissues. We separately collected *B. cinerea*-infected *Arabidopsis* tissues from "annular edge area" (where the plant cells remained alive and a limited amount of *B. cinerea* hyphae were growing within apoplastic spaces) and "central lesion area" (where the plant cells already died and a high density of hyphae were growing) (Fig. 1b), which then were subjected to quantitative real-time PCR (qRT-PCR) analysis of the 15 candidate effector genes. Among them, *BCIN_05g03680*, which has been reported as *B. cinerea* small secreted protein 2 (*BcSSP2*)[32,33], was induced in the infection process and showed the most elevated expression at the edge area (Fig. 1c, d, and Supplementary Fig. 1c), implying a possible role for BcSSP2 in suppressing host defense response for *B. cinerea* infection.

Prediction by SignalP server showed that the N-terminal region (amino acid 1–20) of BcSSP2 has the typical characteristic of secretory signal peptide (Supplementary Fig. 2a), which is essential for effector secretion from pathogens[34]. Yeast secretion assay showed that invertase fused with the BcSSP2 N-terminal signal peptide could be secreted to reduce colorless 2,3,5-triphenyltetrazolium chloride to red formazan, confirming the secretory characteristic of the BcSSP2 N-terminal signal peptide (Fig. 1e and Supplementary Fig. 2b), consistent with previous findings[32]. We further found that Alexa 546-labeled BcSSP2, but not control protein, was located in plant cells when incubated with *Arabidopsis* roots (Fig. 1f), suggesting that BcSSP2 could be internalized by plant cells. Moreover, we used a split GFP system for tracing translocation of pathogen effector in an infection context[35], in which tobacco leaves transiently expressing $GFP_{1\text{-}10}$ (engineered GFP protein consists of strands 1–10 with a specific exclusion of strand 11) was incubated with *B. cinerea* strain containing GFP_{11}-tagged BcSSP2. Notably, GFP signals were accumulated in cytoplasm and nuclei of cells in the edge area of infected leaves (Fig. 1g), validating secretion of BcSSP2 by *B. cinerea* into plant cells. Taken together, these results indicate that BcSSP2 has typical effector features and is translocated into living plant cells.

BcSSP2 contributes to *B. cinerea* virulence

To verify the function of BcSSP2 in *B. cinerea* virulence, we generated *B. cinerea BcSSP2*-knockout mutant strains (termed as *bcssp2-4, bcssp2-10* and *bcssp2-12*) through homologous recombination (Supplementary Fig. 3), and subsequently assessed the virulence of these mutant strains. Disease symptoms caused by the *bcssp2* mutant strains on *Arabidopsis* were significantly attenuated, as indicated by smaller lesions compared with wild-type strain (B05.10) (~55%, 68% and 63% for *bcssp2-4, bcssp2-10* and *bcssp2-12*, respectively) (Fig. 2a, b). To confirm that the reduced virulence was specifically due to the loss of *BcSSP2*, we generated two independent complementation strains (*com-2* and *com-3*) by reintroducing *BcSSP2* gene into the *bcssp2-10* mutant. Real-time PCR analysis confirmed the restored expression of *BcSSP2* in both complemented strains (Supplementary Fig. 4a), and both *com-2* and *com-3* fully rescued the virulence phenotype, resulting in lesion sizes comparable to the wild-type strain (Supplementary Fig. 4b–e). These data collectively demonstrate that *BcSSP2* is required for full virulence of *B. cinerea*.

Since *B. cinerea* has a very broad host range, we further examined the effect of *BcSSP2* on *B. cinerea* virulence in other host plants including lettuce, strawberry and rose. Similarly, the virulence of *BcSSP2* mutants is significantly declined in all tested plant species, indicating a conserved role of BcSSP2 in facilitating *B. cinerea* infection on diverse host plants (Fig. 2c, d).

We then generated transgenic *Arabidopsis* with estradiol-inducible expression of *BcSSP2* (*iBcSSP2*) (Supplementary Fig. 5) to further verify the BcSSP2 function in *B. cinerea* pathogenicity. Estradiol treatment led to more severe disease symptoms in *iBcSSP2* plants but not in the control wild-type (WT) plants upon *bcssp2* strain infection, as indicated by increased *B. cinerea* biomass (~2.1-fold) and plant disease severity (~2.1-fold dead plants) (Fig. 2e, f), demonstrating that the ectopic overexpression of *BcSSP2* promotes plant susceptibility to *B. cinerea* infection. These data further define BcSSP2 as an effector secreted by *B. cinerea* into host cells to promote its virulence.

BcSSP2 interacts with NUP62 and partitions into NUP62 condensates

As BcSSP2 is translocated into plant cells, we wondered whether BcSSP2 targets some protein(s) in plant cells to suppress host immunity. To test this hypothesis, we screened potential BcSSP2 targets from a panel of over a dozen plant proteins known to participate in defense against *B. cinerea*, including coronatine insensitive 1, ethylene insensitive 2, transcription factor WRKY33, and nucleoporins using luciferase (LUC) complementation-imaging (LCI) assay. Intriguingly, strong LUC activity was detected when BcSSP2 was co-expressed with all the components of the center barrier of nuclear pore complex (NUP62, NUP58, NUP54), but not with other nuclear pore components such as NUP88 and NUP96 (Fig. 3a and Supplementary Fig. 6a, b). Such interaction was verified by co-immunoprecipitation (Co-IP) assay in tobacco leaves transiently co-expressing Flag-NUP62 and BcSSP2-GFP (Fig. 3b), and by pull-down assay using purified GST-NUP62 and BcSSP2-His proteins (Fig. 3c). Moreover, BcSSP2 could co-localize with NUP62 in the nuclear envelop (Supplementary Fig. 6c). These results collectively suggest that the effector BcSSP2 targets plant NPC central barrier.

Furthermore, we identified the responsible domain of NUP62 for its interaction with BcSSP2. We truncated NUP62 into a C-terminal domain (CTD) harboring the coil-coil motif and an N-terminal domain

https://doi.org/10.1038/s41467-025-63632-7

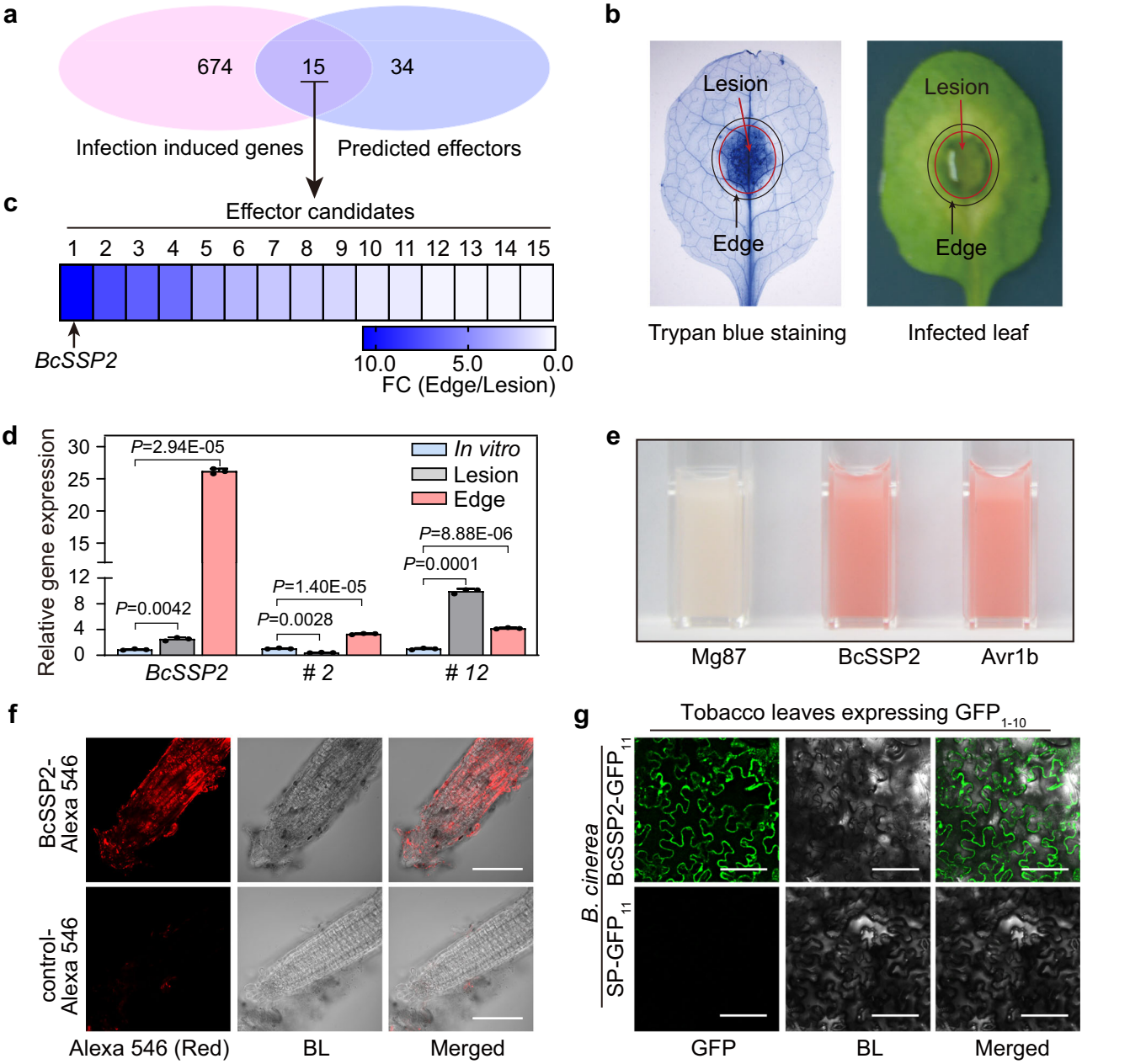

Fig. 1 | BcSSP2 is an effector protein. a Venn diagram shows the overlap of *B. cinerea* genes which are upregulated during infection and predicted to encode putative effectors. The 15 overlapping genes were shortlisted as effector candidates. **b** The lesion area and edge area of *Arabidopsis* leaves infected by *B. cinerea*. A representative *B. cinerea*-infected leaf (48 hpi) with trypan blue staining shows the hyphae and plant cells in the edge and lesion area. **c** Heatmap represents fold change (FC) of expression levels of 15 effector candidates in the edge area relative to the lesion area in *B. cinerea*-infected leaves. The effector candidate with the most elevated expression (namely effector candidate # 1, designated *BcSSP2*) was selected for further study. **d** qRT-PCR analysis on the expression levels of *BcSSP2* in the in vitro culture, the edge or lesion area of *B. cinerea* infection in *Arabidopsis* leaves. Candidates *# 2* and *# 12* serve as the controls. Data are mean ± SD ($n = 3$). Statistical significance was determined by two-sided Student's *t* test. **e** Yeast YTK12 strain carrying SUC2 invertase (fused with the signal peptide of BcSSP2) reduces 2,3,5-triphenyltetrazolium chloride to red formazan, indicating invertase secretion. Mg87 and Avr1b serve as the negative and positive controls, respectively. See also Supplementary Fig. S2B. **f** Entry of BcSSP2 protein into *Arabidopsis* root cells. *Arabidopsis* root tips were incubated with Alexa 546-labeled BcSSP2 or control protein (TrxA-His) for 12–16 h, and then washed 4 times before imaging. Scale bar: 100 μm. BL bright light. **g** BcSSP2 is translocated into host cells in the infection process. Tobacco leaves expressing GFP_{1-10} (engineered GFP protein consists of strands 1–10 with a specific exclusion of strand 11) for 24 h were then drop-inoculated with *B. cinerea* expressing GFP_{11} tagged BcSSP2 (BcSSP2-GFP_{11}) or signal peptide of BcSSP2 (SP-GFP_{11} serves as a control). The edge area was visualized by confocal imaging at 24 hpi for effector translocation. Scale bar: 100 μm. BL, bright light. Source data are provided as a Source Data file.

(NTD) containing the FG-rich domain. In the pull-down assay, the NTD, but not the CTD, of NUP62 could efficiently pull down BcSSP2 (Fig. 3d), indicating that NUP62 interacts with BcSSP2 via its NTD.

As the central barrier undergoes phase separation to form condensates in vitro through the NTD[12], we investigated whether BcSSP2 partitions into NUP62 condensates. BcSSP2, but not the control protein, could efficiently partition into NUP62 condensates when incubated with NUP62 (Fig. 3e and Supplementary Fig. 7a, b). Meanwhile, BcSSP2 was unable to undergo phase separation alone (Supplementary Fig. 7c). These results further verify the interaction between BcSSP2 and NUP62, and suggest that BcSSP2 is able to interact with NUP62 in its phase-separated conformation.

https://doi.org/10.1038/s41467-025-63632-7

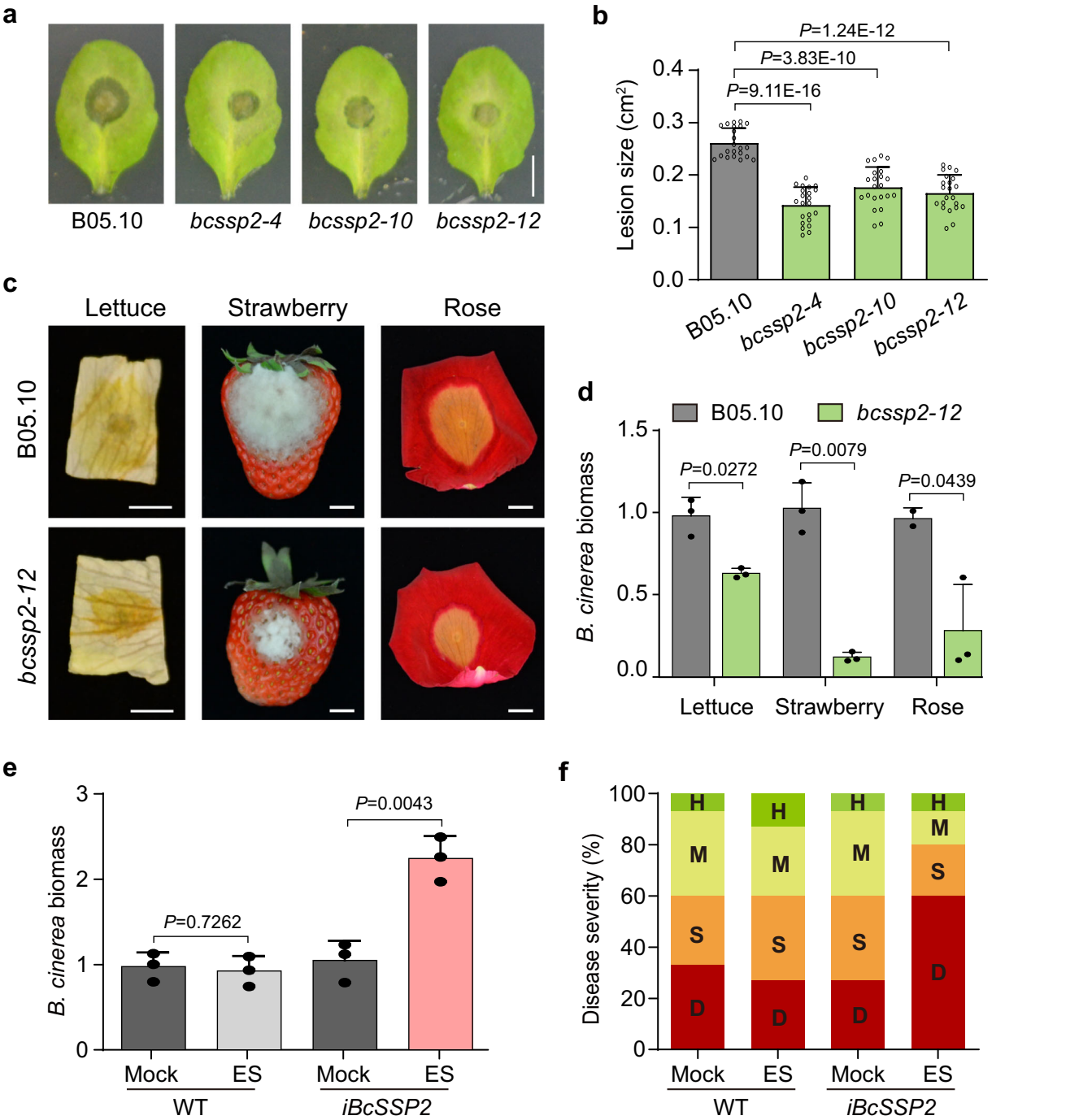

Fig. 2 | BcSSP2 contributes to *B. cinerea* pathogenicity. a, b Knockout of *BcSSP2* in *B. cinerea* reduces its virulence on *Arabidopsis*. Detached WT *Arabidopsis* leaves were inoculated with conidiospores of three independent *BcSSP2* knockout strains (*bcssp2-4*, *bcssp2-10* and *bcssp2-12*), or B05.10. The representative leaves at 48 hpi (**a**) and quantification data of lesion sizes (**b**) are shown. Data are mean ± SD ($n = 22$). Statistical significance was determined by two-sided Student's *t* test. Scale bar: 0.5 cm. **c, d** The *bcssp2* knockout strains show compromised virulence in vegetable (lettuce), fruit (strawberry) and flower petal (rose). The phenotype (**c**) and *B. cinerea* biomass (**d**) are shown. Photos were taken at 3 dpi for lettuce, 4 dpi for strawberry and rose. Data are mean ± SD ($n = 2$ for B05.10-infected rose and $n = 3$ for other groups). Statistical significance was determined by two-sided Student's *t* test. Scale bar: 1 cm. **e, f** Ectopic expression of *BcSSP2* in *Arabidopsis* plants promotes *B. cinerea* infection. The *iBcSSP2* plants and WT plants were treated with estradiol (ES) or DMSO (Mock) and sprayed with conidiospores of *bcssp2-12*. The susceptibility of infected plants at 36 hpi was quantitatively evaluated by *B. cinerea* biomass (**e**) and disease severity (**f**). For (**e**), data are mean ± SD ($n = 3$). Statistical significance was determined by two-sided Student's *t* test. For (**f**), disease severity is classified into four grades: healthy (H, green), mild symptoms (M, pale green), severe symptoms (S, yellow) and completely dead plants (D, red). Source data are provided as a Source Data file.

BcSSP2 interferes with NUP62 phase separation

Since BcSSP2 interacts with the NTD of NUP62 (Fig. 3d) and NUP62 phase separation is crucial for host defense against *B. cinerea*[12], we wonder whether BcSSP2 affects NUP62 phase separation to facilitate *B. cinerea* infection. To address this question, we first tested whether BcSSP2 disturbs phase separation of NUP62 in vitro. We found that the formation of NUP62 condensates was disturbed significantly when incubated with BcSSP2 (Fig. 4a, b).

https://doi.org/10.1038/s41467-025-63632-7

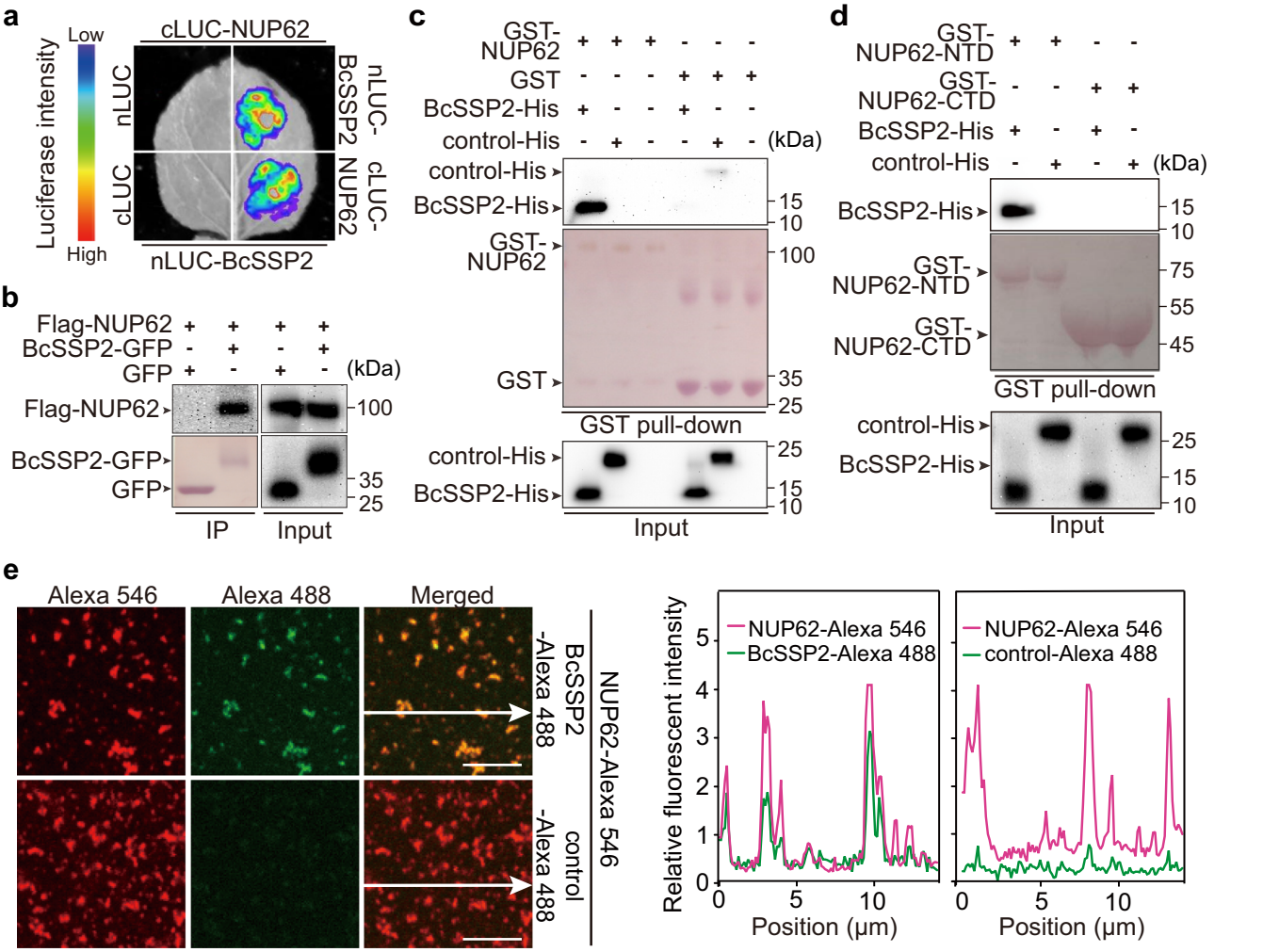

Fig. 3 | BcSSP2 interacts with NUP62 and partitions into NUP62 condensates. **a**–**d** BcSSP2 interacts with NUP62. **a** Luciferase activity was detected at 36 hpi in the LCI assay. **b** Flag-NUP62 and BcSSP2-GFP were transiently expressed in tobacco leaves and immunoprecipitated with GFP trap in the Co-IP assay. Total extracts (Input) and the immunoprecipitates (IP) were analyzed by immunoblots. **c**, **d** Immobilized GST-NUP62, GST-NUP62-NTD and GST-NUP62-CTD were used to pull down BcSSP2-His. TrxA-His (control-His) serves as a negative control for BcSSP2-His. Ponceau S staining indicates the loading of bait proteins. **e** BcSSP2 partitions into NUP62 condensates. Confocal image of NUP62-Alexa 546 with BcSSP2-Alexa 488 (TrxA-Alexa 488 serves as a control) and fluorescent intensity along the arrows are shown, respectively. Scale bar: 5 μm. Source data are provided as a Source Data file.

Furthermore, we used atomic force microscopy (AFM) to characterize the impact of BcSSP2 on the mechanical properties of NUP62 hydrogel which is formed through phase separation. The hydrogels constituted of NUP62 alone, NUP62 with BcSSP2 or NUP62 with control protein, were prepared and subjected to AFM analysis. We measured the stiffness of the hydrogels at multiple points, which is indicated by Young's modulus. The stiffness of NUP62 + BcSSP2 hydrogel decreased dramatically (by about 67% in Median and 70% in Mean of Young's modulus) compared with that of NUP62 alone or NUP62+control hydrogels (Fig. 4c, d), suggesting that BcSSP2 evidently modifies the property of NUP62 hydrogels. Taken together, these results demonstrate that BcSSP2 interferes with NUP62 phase separation in vitro.

To gain insights into the effect of BcSSP2 on NUP62 phase separation in vivo, we inoculated B05.10 strain or *bcssp2-12* mutant strain onto tobacco leaves transiently expressing *NUP62-GFP* for confocal imaging. In the *bcssp2*-infected edge area, the total fluorescent intensity of NUP62 condensates was significantly higher (~1.4-fold) compared with that of B05.10-infected edge area (Fig. 4e, f) while the overall protein level of NUP62 presented no significant difference (Supplementary Fig. 8a). Consistently, estradiol-induced BcSSP2 reduced NUP62 condensates by 81% in tobacco expressing *NUP62-GFP*, with no change of NUP62 total protein level (Fig. 4g, h, and Supplementary Fig. 8b, c). These results collectively demonstrate that BcSSP2 suppresses the phase separation of NUP62 in vivo.

Homologs of BcSSP2 in necrotrophic ascomycetes interfere with NUP62 phase separation

Phylogenetic analysis showed that BcSSP2 homologs were widely distributed among ascomycetes and highly conserved in necrotrophic ascomycetes (Supplementary Fig. 9a). Representative analysis of the BcSSP2 homologs from *S. sclerotiorum* (a broad host range necrotrophic pathogen that causes one of the most prevalent diseases in oilseed rape) and *Aspergillus flavus* (an extremely common fungal pathogen that produces carcinogenic aflatoxins in the infected crops) showed that the SsSSP2 (*S. sclerotiorum* SSP2) and AfSSP2 (*A. flavus* SSP2) were able to interact with NUP62 (Supplementary Fig. 9b), indicating an evolutionarily conserved strategy adopted by various necrotrophic ascomycetes to secret BcSSP2-like effectors that target plant NPCs to facilitate pathogen infection.

Furthermore, we wondered if SsSSP2 and AfSSP2 suppress NUP62 phase separation. To test this hypothesis, *NUP62-GFP* together with estradiol-inducible *SsSSP2* (*iSsSSP2*) or estradiol-inducible *AfSSP2* (*iAfSSP2*) were transiently co-expressed in tobacco leaves for NUP62

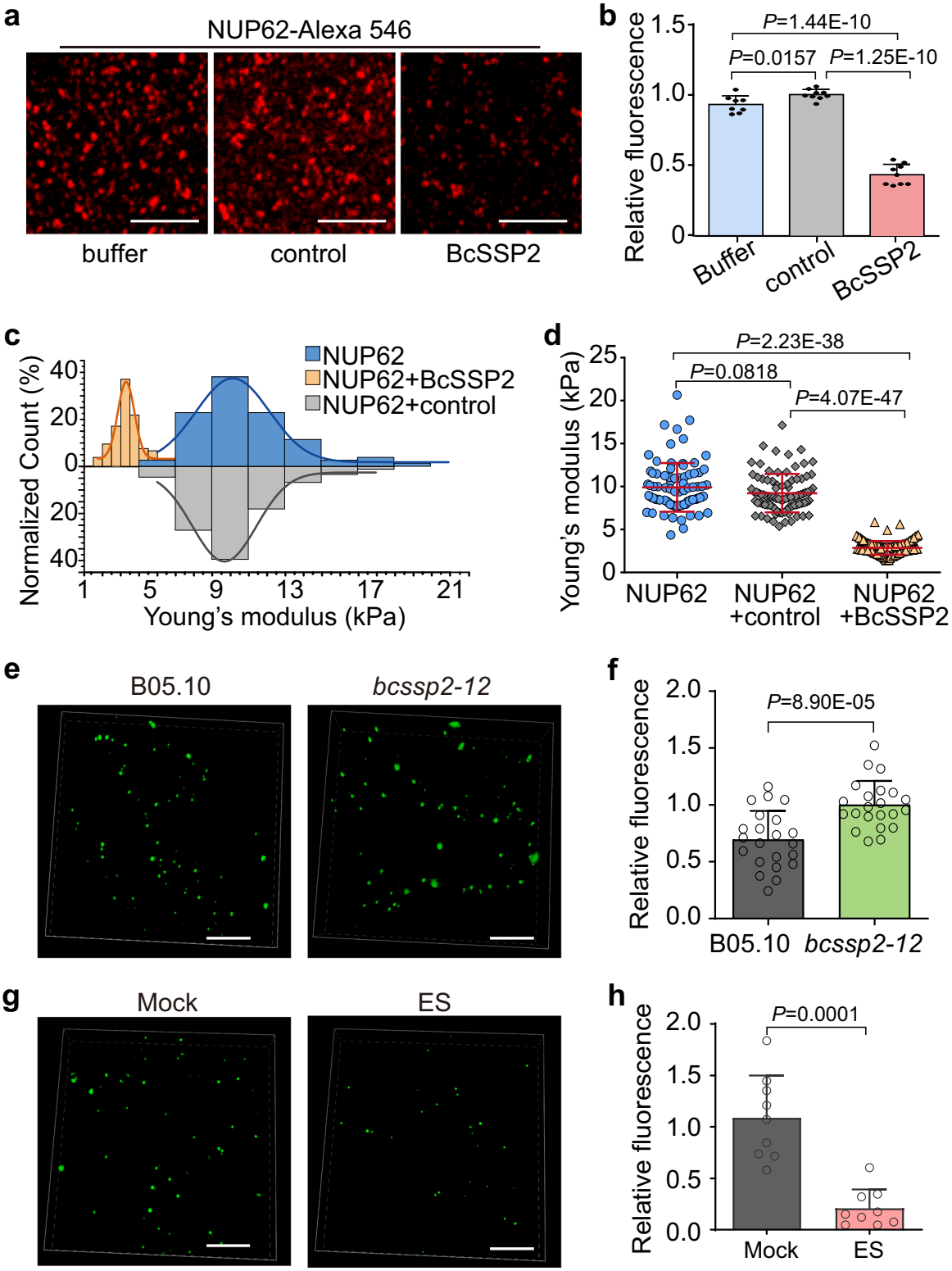

puncta observation. The formation of NUP62 condensate decreased evidently with estradiol-induced expression of *SsSSP2* and *AfSSP2*, respectively (Supplementary Fig. 10a, b). Meanwhile, the protein abundance of NUP62 presented no significant difference without (Mock) or with estradiol provision (ES) (Supplementary Fig. 10c). Thus, SsSSP2, as well as AfSSP2, could interfere with NUP62 phase separation, suggesting a conserved feature of necrotrophic BcSSP2-like effectors for interfering with the phase separation of NPC central barrier.

BcSSP2 attenuates the NUP62 phase separation-dependent nuclear transport of MPK3

As phase separation of the NPC central barrier mediates selective nucleocytoplasmic transport which is facilitated by the nuclear transport receptor (NTR)[12], we next investigated whether BcSSP2-mediated perturbation on NUP62 phase separation affects the selective nucleocytoplasmic transport. Firstly, we adopted in vitro hydrogel transport assay to detect the influence of BcSSP2 on the transport efficiency of NUP62 using the surface-redesigned GFP protein (GFP8W,

Fig. 4 | BcSSP2 interferes with NUP62 phase separation. a, **b** BcSSP2 interferes with NUP62 condensates formation. The representative photos (**a**) and relative fluorescent intensity (**b**) of 2 μM NUP62 incubated with BcSSP2, control protein (TrxA-His) or equal volume buffer are shown. 40 μM BcSSP2 or control protein was used. Data are mean ± SD ($n = 8$ for buffer, and $n = 9$ for control and BcSSP2). Statistical significance was determined by two-sided Student's t test. Scale bar: 5 μm. **c**, **d** BcSSP2 modifies stiffness of NUP62 hydrogel. 1 mM NUP62 without (NUP62 alone) or with 0.1 mM BcSSP2 (NUP62 + BcSSP2), or with 0.1 mM TrxA-His (NUP62 + control, TrxA-His served as a control) were subjected to hydrogel formation, respectively. The stiffness of hydrogels was determined by AFM and indicated as Young's moduli. Medians (**d**) obtained from GaussAmp simulation and means (**c**) are shown. Data are mean ± SD ($n = 83$ for NUP62, $n = 89$ for NUP62 + control, $n = 112$ for NUP62 + BcSSP2). Statistical significance was determined by two-sided Student's t test. **e**, **f** Infection by B05.10 suppresses NUP62 condensates formation compared with infection by *bcssp2-12* in vivo. Tobacco leaves expressing NUP62-GFP for 24 h were subsequently infected with *bcssp2-12* or B05.10 strains for 24 h, and the edge area of the infected leaves was subjected for confocal imaging (**e**) and relative fluorescent intensity analysis (**f**). Data are mean ± SD ($n = 22$). Statistical significance was determined by two-sided Student's t test. Scale bar: 10 μm. **g**, **h** Ectopic expression of BcSSP2 suppresses NUP62 condensates formation. NUP62-GFP and iBcSSP2 were co-expressed in tobacco leaves. Estradiol (ES) or DMSO (Mock) was applied 6 h before confocal imaging (**g**) and relative fluorescent intensity analysis (**h**). Data are mean ± SD ($n = 9$). Statistical significance was determined by two-sided Student's t test. Scale bar: 10 μm. Source data are provided as a Source Data file.

eight amino acids located in GFP surface were mutated to tryptophans) to mimic the NTR-mediated selective transport[36]. The translocation speed of MBP-GFP8W in NUP62 + BcSSP2 hydrogel decreased by nearly half, compared with that of NUP62 or NUP62+control hydrogel (Fig. 5a, b). Consistently, the translocation speed of MBP-GFP8W in NUP62 hydrogel pre-incubated with BcSSP2 was obviously decreased (Supplementary Fig. 11), suggesting that BcSSP2 attenuates the NUP62 phase separation-mediated MBP-GFP8W transport.

Since phase separation of the NPC central barrier mediates nuclear import of defense-related cargo MPK3[12], we then tested whether BcSSP2 suppresses MPK3 nuclear transport. The in vitro assays showed that the partition of MPK3 (with *Arabidopsis* crude extracts) in NUP62 hydrogel was significantly inhibited by BcSSP2 (Fig. 5c, d). As assayed in vivo, nuclear proportion of MPK3 in plants infected by wild-type *B. cinerea* B05.10 was obviously lower (by ~61.5%) in comparison with that infected by *BcSSP2* knockout strain *bcssp2-12*, though the overall amount of MPK3 kept unchanged in plants infected by either B05.10 or *bcssp2-12* (Fig. 5e, f). In line with nuclear attenuation of MPK3, the expression level of defense marker gene *PDF1.2* was significantly decreased (~50%) in B05.10-infected plants compared with that of *bcssp2*-infected plants (Fig. 5g). These results suggest that BcSSP2 of *B. cinerea* B05.10 inhibits nuclear transport of MPK3 in plant cells during pathogen infection.

Moreover, the ectopic expression of *BcSSP2* in *Arabidopsis* plants significantly suppressed MPK3 nuclear transport. Though the total MPK3 protein level presented no discernible difference (Fig. 5h), the nuclear accumulation of MPK3 was remarkably impaired by 67% in estradiol-treated *iBcSSP2* transgenic plants (Fig. 5i). Constantly, the expression level of *PDF1.2* was declined by 88% in estradiol-treated *iBcSSP2* transgenic plants (Fig. 5j).

Taken together, our results in Figs. 1–5 suggest that BcSSP2, secreted by *B. cinerea* into host cells, targets the NPC central barrier, interferes with its phase separation and consequently attenuates phase separation-dependent nucleocytoplasmic transport of MPK3, to suppress plant defense response for effective pathogen infection (Fig. 6).

Discussion

Pathogens and their hosts are inevitably involved in endless arms race, while effector proteins act as the key weapons in pathogens' arsenal[3,17–20]. Previous studies uncovered various strategies used by pathogen effectors to combat host defense response, such as altering the expression of host genes[21,22], suppressing the host small RNA-based gene silencing[26,31], and interfering the degradation of host proteins[24]. The phase separation of effector protein has recently emerged as a novel strategy for pathogens to interfere with host defense response[37]. In this study, we identify an effector from a plant pathogen that, rather than undergoing phase separation itself, suppresses host phase separation-mediated defense processes to promote infection. These findings highlight phase separation as a new and critical battleground in pathogen-host interactions.

NPC serves as the sole exchange channel between nucleus and cytoplasm[38,39], and plays important roles in diverse biological processes[40–44]. We previously showed that the integrity of NPC central barrier is required for plant defense and that the NPC central barrier undergoes phase separation to facilitate the active transport of cargoes essential for plant defense[12]. In the current study, we further report a pathogen effector, BcSSP2, that targets plant NPCs. BcSSP2 binds to FG-nucleoporins of the central barrier and interferes with their phase separation to disrupt nucleocytoplasmic transport of important immune regulators, including MPK3, to inhibit host defense for effective pathogen infection. In addition to MPK3, the nucleocytoplasmic transport of other immune components involved in resistance to *B. cinerea* may also be affected, a possibility that warrants further investigation. These data support the notion that phase separation of NPC central barrier is crucial for plant defense as demonstrated in our previous work[12], and further uncover that some pathogens encode specific effectors that can interfere with phase separation of host NPCs to promote infection.

B. cinerea is one of the most devastating plant pathogens, which has a broad host range[27], and causes huge economic losses worldwide. Direct killing host cells with the secreted lytic enzymes, oxalic acid and phytotoxins were thought to be the major infection strategies adopted by *B. cinerea*[28]. Recent studies revealed that *B. cinerea* secrets small RNAs into plant cells to suppress RNAi-based plant defense response for successful infection[31]. Here, we found that *B. cinerea* secrets BcSSP2 to attenuate phase separation of plant NPC to suppress host defense response for effective pathogen invasion. Previous studies have shown that the phase separation of NUP62 is mediated by weak, multivalent hydrophobic interactions among its N-terminal FG repeat domains[12]. Consistently, our results demonstrate that BcSSP2 interacts with the N-terminal region of NUP62 (Fig. 3d), suggesting that BcSSP2 may disrupt NUP62 phase separation by interfering with FG-FG interactions of NUP62. Elucidating the precise mechanism by which BcSSP2 interferes with NUP62 condensate formation will pave the way for engineering the nuclear pore complex to enhance plant resistance against *B. cinerea*.

Interestingly, previous studies have revealed that prolonged ectopic expression of BcSSP2 or infiltration of a physiological relevant concentration of purified BcSSP2 proteins in plant tissues could cause chlorosis and slow development of cell death (visible around 15 days after agroinfiltration/treatment)[32,33], which differs from typical CDIPs (cell death inducing proteins) that induce instant cell death (within 5 days). It was hypothesized that BcSSP2 protein might not cause direct damage to the plant cell but affect some unknown pathways that eventually lead to cell death[32]. Considering the crucial function of NPC in plant cell physiology, our work provides a possible mechanistic explanation (e.g., through inhibiting plant NPC function) for the previously reported slow phytotoxicity of BcSSP2. However, it is also plausible that BcSSP2 may target other components beyond NPC to induce slow plant cell death, as pathogen effectors are known to promote infection with multiple mechanisms[19].

https://doi.org/10.1038/s41467-025-63632-7

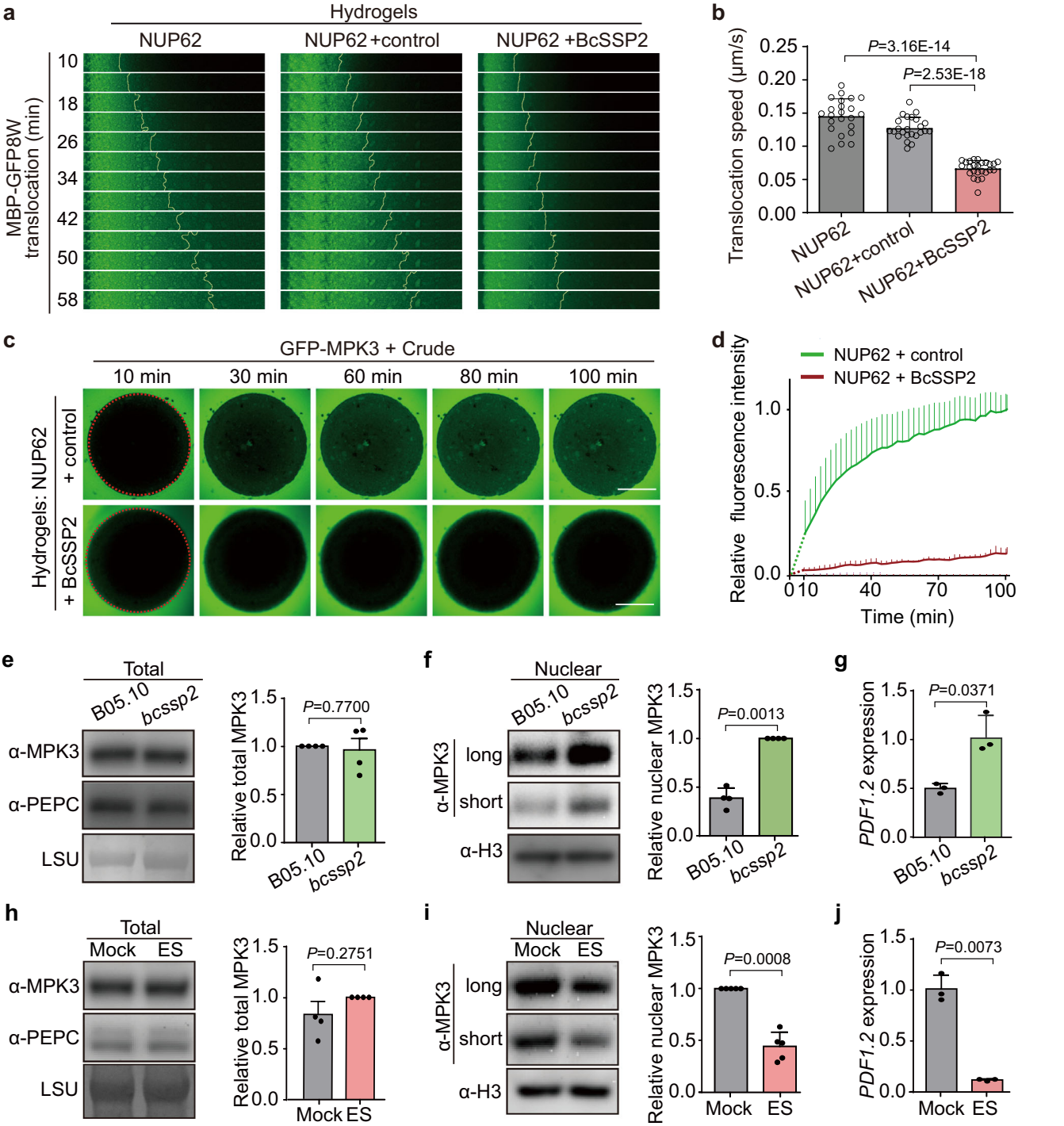

Fig. 5 | BcSSP2 suppresses NUP62 phase separation-mediated selective nucleocytoplasmic transport. a, **b** BcSSP2 inhibits MBP-GFP8W translocation into NUP62 hydrogel. Time-lapse photos were taken since MBP-GFP8W was supplied. The representative photos (**a**) and the translocation speeds (**b**) of MBP-GFP8W in NUP62, NUP62+control and NUP62 + BcSSP2 hydrogels are shown. Data are mean ± SD ($n = 23$ for NUP62, $n = 24$ for NUP62+control, $n = 25$ for NUP62 + BcSSP2,). Scale bar: 100 μm. **c**, **d** BcSSP2 inhibits MPK3 translocation. Time-lapse photos were taken since GFP-MPK3 was supplied. Representative photos (**c**) and relative fluorescent intensity (**d**) of GFP-MPK3 in NUP62+control or NUP62 + BcSSP2 hydrogels with WT *Arabidopsis* (Col-3) crude extracts are shown ($n = 3$). Dotted circles mark the hydrogel edge. Scale bars: 500 μm. **e**–**j** BcSSP2 suppresses nuclear accumulation of MPK3. For (**e**–**g**) WT *Arabidopsis* plants infected by B05.10 or *bcssp2-12* at 36 hpi were subjected to analysis of total MPK3 proteins (**e**), nuclear MPK3 proteins (**f**) and *PDF1.2* transcripts (**g**). For (**h**–**j**), the *iBcSSP2* plants were treated with estradiol (ES) or DMSO (Mock), and then inoculated with *bcssp2-12* knockout strain for 36 h and subjected to analysis of total MPK3 proteins (**h**), nuclear MPK3 proteins (**i**) and *PDF1.2* transcripts (**j**). The protein levels of MPK3 were quantified based on the relative intensity of protein bands while the max intensity was normalized to 1 (**e**, **f**, **h** and right panel of **i**). The bands of MPK3 in (**f**) and (**i**) are presented with a short or long exposure time. Data are mean ± SE ($n = 4$ in (**e**, **f**, **h**) and $n = 5$ in (**i**), or mean ± SD ($n = 3$ in (**g**, **j**)). PEPC (phosphoenolpyruvate carboxylase), LSU (large subunit of rubisco protein) and H3 (Histone H3) serve as loading controls. MPK3 and PEPC were run on the same gel with the membrane cut for different antibodies; LSU was stained after exposure in (**e** and **h**). MPK3 and H3 were run on the same gel with the membrane cut for different antibodies in (**f** and **i**). Statistical significance was determined by two-sided Student's *t* test. Source data are provided as a Source Data file.

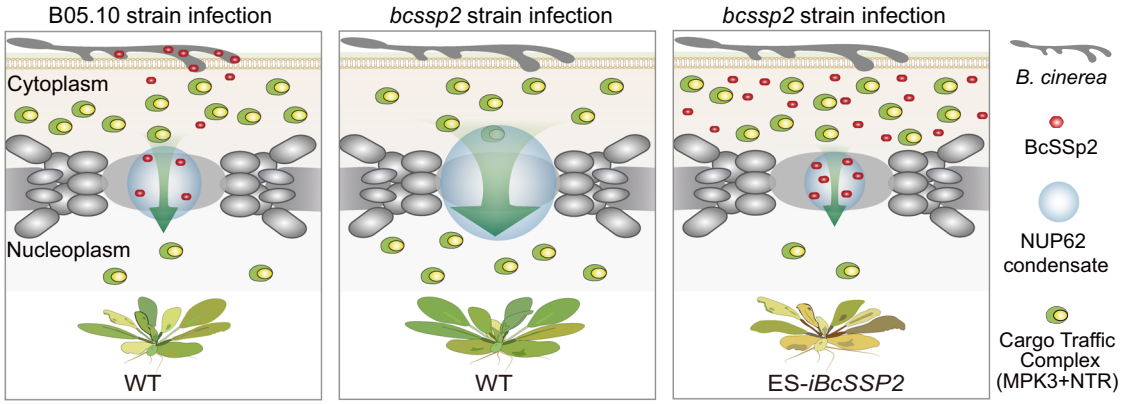

Fig. 6 | A simplified model for BcSSP2 action. Upon *B. cinerea* infection, WT plants accumulate immune regulator MPK3, which is transported from cytoplasm into nucleus via NPC central barrier phase separation to activate expression of downstream genes essential for plant resistance. To combat plant immunity, *B. cinerea* (B05.10 wild-type strain) accumulates BcSSP2 and secrets it into the plant cells of the edge area to target plant NPC central barrier (NUP62, NUP58 and NUP54), disrupt their phase separation (NUP62 is representatively indicated), and attenuate NTR-aided nuclear transport of MPK3, thereby suppressing plant defense responses for effective pathogen infection (as indicated by an infected plant) (first panel). When infected by the *bcssp2* mutant, the NPC phase separation-mediated defense response of WT plants is not suppressed due to the absence of BcSSP2, which allows efficient nuclear transport of MPK3 essential for plant defense (a healthy plant) (second panel). However, NPC phase separation-mediated plant defense responses are suppressed by the ectopically expressed BcSSP2 in estradiol-treated *iBcSSP2* transgenic plants (ES-*iBcSSP2*), which leads to attenuated plant defense and severe disease symptoms (a susceptible plant) (third panel).

As BcSSP2 homologs are widely distributed among ascomycetes (Supplementary Fig. 9a), an evolutionarily conserved strategy might be evolved by these necrotrophic pathogens to facilitate their colonization and infection. It would be exciting to explore whether targeting the NPC central barrier is a general mechanism evolved by necrotrophic pathogens to suppress the NPC phase separation-mediated host defense response for their effective invasion.

Methods

Plants

Arabidopsis thaliana ecotype Col-0 was used as wild-type (WT) control. To generate the transgenic plant *iBcSSP2*, *BcSSP2* CDS region was cloned into *pER8*, whose expression was driven by an estradiol-inducible promoter, and then transformed into WT plants using the Agrobacterium-mediated floral dip method. Seeds were sterilized with bleach buffer (20% [v/v] bleach, 0.1% [v/v] triton-100), washed with sterile water, and chilled at 4 °C in dark for 3 days. After vernalization, seeds were plated on MS medium (Murashige and Skoog medium, Sigma-Aldrich), and then cultured in a growth room (22 °C with a 16 h/8 h light/dark photoperiod, long day, LD). 8-day-old seedlings were transplanted into soil and grown under the same condition. For pathogen inoculation, plants were grown in soil for 3 to 4 weeks at 22 °C with a 10 h/14 h light/dark photoperiod (short day, SD).

Nicotiana benthamiana (*N. benthamiana*) seedlings were grown at 22 °C with a 16 h/8 h light/dark photoperiod.

Botrytis cinerea

The wild-type *Botrytis cinerea* (*B. cinerea*) strain B05.10 was previously described[45]. PDA medium (Potato Dextrose Agar medium, BD) was used to cultivate *B. cinerea* at 22 °C.

B. cinerea inoculation

Conidiospores were collected from *B. cinerea* plates and diluted to 1×10^6 conidiospores/mL in PDB medium (Potato Dextrose Broth, BD). For drop-inoculation assay, 5 μL conidiospores were dripped on the central of detached leaves, and the inoculated leaves were kept in high humidity for 48 h and photographed for lesion size measurement. For spray-inoculation assay, the transgenic plants *iBcSSP2* and WT plants were transplanted into MS medium supplemented with 1 μM estradiol or mock (0.002% DMSO) for 24 h, and then sprayed evenly with *B. cinerea* conidiospores. The inoculated seedlings were kept in high humidity for 36 h. The disease severity was classified into four grades: healthy (H, green), light symptoms (L, pale green), severe symptoms (S, yellow), or completely dead (D, red). For *B. cinerea* biomass detection, quantitative real-time PCR (qRT-PCR) was applied with primers for *B. cinerea*-specific *ITS* gene and *Actin* of the responding hosts (*Arabidopsis*, lettuce, strawberry and rose) served as internal control (Supplementary Data 4).

Construction of *B. cinerea* mutants and complementation strains

To generate *B. cinerea* knockout mutants, ~600 bp upstream and downstream flanking sequences of *BcSSP2* were cloned into pLOB7 which carrying a hygromycin B resistance cassette as a selectable marker. The resulting plasmids were introduced into *B. cinerea* protoplasts prepared by enzymatic digestion of young mycelia with lysing enzymes. Protoplast transformation was performed using polyethylene glycol (PEG)-mediated transfoamation[46]. Transformants were selected with hygromycin and confirmed by PCR amplification. Primers are listed in Supplementary Data 4.

For complementation, the coding sequence of *BcSSP2* were amplified from B05.10 cDNA and cloned into the pNAN-OGG vector, where it was placed under the control of the fungal Polic promoter and linked to nourseothricin resistance. The resulting plasmid was amplified, and the PCR products were used to transform the *bcssp2-10* mutant strain. The transformants were initially selected on nourseothricin-containing plates and subsequently verified by PCR-based genotyping. All primer pairs are listed in Supplementary Data 4.

BcSSP2 signal peptides validation

Functional validation of BcSSP2 predicted signal peptides was conducted using the yeast secretion system[47]. The coding sequence of BcSSP2 signal peptide (1-20Aa, SP) was cloned into *pSUC2* vector to generate *pSUC2-BcSSP2SP*, in which the SP of BcSSP2 was fused with truncated SUC2 invertase lacking its original SP. *pSUC2-BcSSP2SP*, *pSUC2-Mg87* and *pSUC2-Avr1b*[48] were transformed into yeast strain YTK12 (SUC2-minus), respectively. The transformants were selected by CMD-W plates (0.67% [v/v] yeast nitrogen base without amino acids, 2% [v/v] sucrose, 0.1% [v/v] glucose, 0.075% [v/v] tryptophan dropout supplement, and 2% [v/v] agar). The selected transformants were then coated on YPRAA plates (1% [v/v] yeast extract, 2% [v/v] peptone, 2% [v/v] raffinose, 2 μg/L Antimycin A and 2% [v/v] agar),

only strains with secreting SUC2 invertase could consume raffinose and grow well.

Invertase secretion was also confirmed with 2,3,5-triphenyltetrazolium chloride (TTC) assay since invertase could reduce colorless TTC to red-colored 2,3,5-triphenylformazan. Transformants cultured in liquid medium were collected. After washing, the transformants were resuspended in sterile water. Subsequently, 0.1% [v/v] TTC was added into the transformants suspension, and the mixture was incubated at 35 °C for 30 min. The resulting mixture was transferred into cuvettes for photographing.

Effector internalization assay

For the root incubation assay, about 1 cm root tips were detached from plate-grown *Arabidopsis* Col-0 seedlings and incubated with 50 μM Alexa 546-labeled effector BcSSP2 or TrxA-His (negative control). After incubation for 12–16 h at 23 °C, the roots were washed 4 times with MS medium before confocal imaging[49].

For the GFP strand assay[35], BcSSP2 or signal peptide of BcSSP2 (SP, negative control) were tagged with the 11th strand of GFP and transformed into *Botrytis cinerea* strain B05.10 to generate the transgenic stain BcSSP2-GFP_{11} or SP-GFP_{11}. Tobacco expressing $GFP_{1\text{-}10}$ (strands 1–10) for 24 h were infected with the transgenic stain BcSSP2-GFP_{11} and SP-GFP_{11}. The edge area of the infected leaves (24 hpi) was subjected to confocal imaging.

N. benthamiana transient expression

Freshly cultured *Agrobacterium* was collected and resuspended in infiltration buffer (10 mM MES, 10 mM $MgCl_2$, 0.2 mM acetosyringone) and kept in dark for 3 h. Leaves of 4-week-old *N. benthamiana* plants were infiltrated with indicated combinations of Agrobacterium strains. Plants were maintained at 22 °C for 36 h before LCI and subcellular localization assay, respectively. In the assay to detect BcSSP2, SsSSP2 and AfSSP2 effect on NUP62 phase separation, discs of *N. benthamiana* detached leaves were soaked in 10 μM estradiol or mock buffer (0.02% [v/v] DMSO) for 6 h to induce BcSSP2, SsSSP2 and AfSSP2 expression before confocal imaging.

Co-IP assay

Total proteins were extracted from 5 to 10 g *N. benthamiana* leaves co-expressing indicated protein combinations with extraction buffer (50 mM Tris·HCl, pH 7.5, 150 mM NaCl, 0.5% [v/v] Triton X-100, 0.5% [v/v] Nonidet P-40, 10 μM MG132, 0.1 mM PMSF, Roche inhibitor cocktail). After centrifugation at 16,000 × *g*, 4 °C for 10 min to remove the debris, 20 μL of pre-washed anti-GFP magnetic agarose beads (GFP-TrapMA, Chromo Tek) were added to the supernatants. The mixture was incubated for 4 hours at 4 °C. The beads were then washed with extraction buffer for 5 times, and the precipitated proteins were eluted by boiling with SDS loading buffer for 5 min. The final samples were analyzed by Western Blot. The concentrated total proteins before adding anti-GFP beads were also detected for indicating the amount of the total input proteins. For Western blotting, anti-Flag (Abmart, M20008, 2000-fold dilution) and Mouse monoclonal anti-GFP (Abmart, M20004, 2000-fold dilution) were used.

In vitro pull-down assay

Purified GST-NUP62, GST-NUP62-NTD, GST-NUP62-CTD and GST proteins were used as baits to incubate with 50 μL pre-washed Glutathione Sepharose 4B affinity chromatography (GST beads, GE Healthcare). 20 μg purified BcSSP2-His and TrxA-His proteins (purified from *pET32a* as control) were incubated with GST-NUP62, GST-NUP62-NTD, GST-NUP62-CTD or GST at 4 °C for 1 h in reaction buffer (20 mM Tris·HCl, pH 7.5, 500 mM NaCl, 10% [v/v] glycerol and 0.1% [v/v] Triton-X 100), respectively. After extensive washing with reaction buffer, the complexes were released from GST beads by boiling with SDS loading buffer for 5 min.

BcSSP2-His and control proteins were detected by Western blot using Anti-His antibody (Anti-His Mouse mAb, Abmart), and GST-NUP62, GST-NUP62-NTD, GST-NUP62-CTD or GST was showed by Ponceau S staining of the polyvinylidene difluoride membranes.

Protein labeling

The purified proteins were labeled by Alexa Fluor 488 carboxylic acid (ThermoFisher) or Alexa Fluor 546 carboxylic acid (ThermoFisher) at room temperature for 1 h. Then, the free dye was removed by illustra™ Microspin G-50 Columns (GE Healthcare). To minimalize the impact of Alexa dye, less than 1% total proteins were labeled to perform partitioning experiments in our study.

Protein condensate assays

Protein condensate assay was performed in the buffer containing 20 mM HEPES, pH7.4, 150 mM NaCl, 10% [v/v] glycerol, 5 mM DTT. For MBP-fused proteins, additional TEV protease (the molar concentration of TEV was 1% of MBP-tagged proteins) was added to the system to cleave MBP-tag during the condensate assembly[50,51]. For detecting the effect of BcSSP2 on NUP62 phase separation, 2 μM NUP62 protein (NUP62 is cleaved from MBP-NUP62 and labeled with Alexa 546) was mixed with 40 μM dye-free BcSSP2 (BcSSP2-His) or control (TrxA-His) protein. For detecting the colocalization of MBP-GFP8W with NUP62 condensate, MBP-GFP8W and MBP-GFP were added to the NUP62 condensate pool. All the experiments were performed on 384-low-binding multi-well 0.17 mm microscopy plates (Cellvis, P384-1.5H-N). The images were captured by a Laser Scanning Confocal Microscopy (Nikon A1R HD25). NIS-Element AR5.2 software was used to analyze the data.

Hydrogel's preparation

Hydrogels were prepared according to previously described procedure[36,52] with some modifications. Purified MBP-NUP62 was precipitated by 4 M $(NH4)_2SO_4$ solution and subjected to resuspension in the 0.1% [v/v] trifluoroacetic acid (TFA) to final concentration about 1 mM. 1 μL protein mixture was dripped on glass bottom dishes (Cellvis) and were allowed for 2 days to complete gelation. For MBP-NUP62 + BcSSP2 or MBP-NUP62+control hydrogels, MBP-NUP62 incubated with BcSSP2 or control protein in 4 °C for 1 h before precipitating with $(NH4)_2SO_4$. The final concentration was 1 mM for MBP-NUP62 and 0.1 mM for BcSSP2 and control protein.

AFM assay

The AFM experiment was performed on the home-built atomic force microscope (AFM)[53]. Prior to each measurement, in situ spring constant and sensitivity of the probe was calibrated in PBS solution. Probe was moved vertically on the top of hydrogels dipping in PBS solution. The force generated by the downward-moving probe was measured. The signal curve of the tip deflection was recorded. The slope value κ (pN/nm) of the approaches curve was analyzed, adjusted with spring constant and sensitivity of the probe. And the Young's modulus *E* (kPa) was calculated. The histograms of the Young's modulus were fitted with Gauss distribution with the model of GaussAmp in OriginPro 9.1 software.

Translocation assay

For assays in the translocation experiments of MBP-GFP8W, MBP-GFP8W (to final concentration of 4 μM) were added into hydrogels of NUP62, NUP62 + BcSSP2 and NUP62 + control. For the translocation experiments of GFP-MPK3, 10 μL target proteins solutions (4 μM GFP-MPK3, 4 μM MBP-GFP, 4 μM GFP-MPK3 along with 10 μg/μL Col-3 plant crude, 4 μM GFP-MPK3 along with 10 μg/μL Col-3 plant crude) were added to cover the hydrogels. For assays in Supplementary Fig. 10, MBP-NUP62 hydrogels were pre-incubated with 8 μM dye-free BcSSP2, control protein

(TrxA-His) or protein storage buffer for 1 h before adding MBP-GFP8W (to final concentration of 4 μM).

After samples loading, images were captured immediately using the Laser Scanning Confocal Microscopy (Nikon A1R HD25). Since sample loading and instrument commissioning (including location marking and samples focusing) are time-consuming, it is hard to capture the first frame within 10 min. Translocation speed was analyzed with NIS-Elements AR. We focused on the bottom of the hydrogel solutions and measured the inside fluorescence of the hydrogels (within dotted circles as shown in the Figure). Half of the mean fluorescence intensity outside the hydrogel was set as the cutoff in the translocation speed assays.

Protein purification

The recombinant vectors (see as Supplementary Data 5) of MBP-NUP62-His, MBP-GFP-His, MBP-GFP8W-His, GFP-MPK3-his, TrxA-His, GST-NUP62, GST-NUP62-NTD and GST-NUP62-CTD were transformed into *Escherichia coli* BL21 (DE3), respectively. The cells were cultured in LB broth (25 μg/mL ampicillin) at 37 °C until they reached at the logarithmic phase (OD_{600} = 0.8). The expression of proteins was induced by 0.5 mM IPTG at 16 °C for 16 h. Then, the cells were harvested through centrifugation at 4000 × *g* for 30 min, and resuspended in lysis buffer (40 mM Tris·HCl, pH 8.0, 500 mM NaCl, 10% [v/v] glycerol), and lysed by ultrasonication before centrifugation (16000 × *g*, 30 min at 4 °C). The target proteins were purified through Ni-NTA Agarose (Thermo Fisher Scientific) for MBP-NUP62-His, MBP-GFP-His, MBP-GFP8W-His, GFP-MPK3-His and TrxA-His, proteins and Glutathione Sepharose 4B affinity chromatography (GE Healthcare) for GST-NUP62, GST-NUP62-NTD and GST-NUP62-CTD. Finally, Gel-filtration chromatography (SD200, Superdex200 Increase 10/300, GE Healthcare) was performed for further purification with the buffer: 20 mM HEPES, pH 7.4, 500 mM NaCl, 10% [v/v] glycerol.

The BcSSP2-His recombinant plasmid (*pFastBac-BcSSP2-His*) was transformed into DH10Bac competent cells to produce recombinant baculovirus of *BcSSP2-His* Bacmid. Subsequently, BcSSP2-His protein was expressed within Sf9 insect cells (Gibco) which were infected by recombinant baculovirus of *BcSSP2-His* Bacmid. After cultured at 28 °C in Sf-900™ II SFM medium for 48 h, the cells were collected and resuspended in the TBS buffer: 20 mM Tris·HCl, pH 8.0, 150 mM NaCl. Cell lysis was centrifuged at 16000 × *g* for 30 min to remove cell debris after sonication. The proteins in the supernatant were purified by Ni-NTA Agarose (Thermo Fisher Scientific) and followed by gel-filtration chromatography (SD200, Superdex200 Increase 10/300, GE Healthcare) for further purification with the HEPES buffer: 20 mM HEPES, pH7.4, 150 mM NaCl.

Each purification step was identified by SDS-PAGE, only the high-quality proteins were concentrated and frozen in liquid nitrogen and stored at −80 °C in storage buffer.

Subcellular fraction assay

Seedlings were harvested and ground to a fine powder in liquid nitrogen. 0.5 g powder was suspended in 3 mL precooled extraction buffer (10 mM Tris·HCl, pH 7.4, 10 mM $MgCl_2$, 10 mM NaCl, 10 mM β-mercaptoethanol, 10% [v/v] glycerol and Roche protease inhibitor cocktail). The homogenate was filtered through double layers of Miracloth twice. The filtrate was spun at 1500 × *g*, 4 °C for 5 min to pellet the nuclei. The supernatant was then centrifuged at 10,000 × *g*, 4 °C for 10 min and the new supernatant was collected as the cytoplasmic fraction. The pellets were washed 7 times with 2 mL of washing buffer consisting of 10 mM Tris, pH 7.5, 10 mM $MgCl_2$, 10 mM NaCl, 1 M hexylene glycol, 0.5% [v/v] Triton X-100, 10 mM β-mercaptoethanol and Roche protease inhibitor cocktail. The final pellets were resuspended in 200 μL 8 M urea and sonicated. The homogenate was centrifuged at 16,000 × *g* for 10 min and 4 °C to remove debris and collected as the nuclear fraction. For Western blotting, the following primary antibodies were used: rabbit polyclonal anti-AtMPK3 (Sigma-Aldrich, M8318; 1000-fold dilution), rabbit polyclonal anti-PEP Carboxylase (Abcam, ab34793; 10000-fold dilution), and rabbit polyclonal anti-Histone H3 (Sigma-Aldrich, H0164; 10000-fold dilution).

Confocal imaging of plant materials

Detached roots and leaf discs were fixed in microslides filling with liquid MS medium. The fluorescence signal was detected on a Nikon A1R HD25 with the galvano scanner. For puncta quantification, the 3D model was used. All the layers with signals were scanned and 30 layers (0.5 μm/layer) with the strongest signals were selected for analysis. Analysis of puncta number and intensity was performed by the software of NIS-Element AR5.2 and the presented images were processed with deconvolution.

In the assay to detect BcSSP2, SsSSP2 and AfSSP2 effect on NUP62 phase separation, discs of tobacco detached leaves were soaked in 10 μM estradiol or mock buffer (0.02% [v/v] DMSO) for 6 h to induce *BcSSP2*, *SsSSP2* and *AfSSP2* expression and then washed 4 times with MS medium before sample loading. In the assay with pathogen infection, tobacco leaves expressing NUP62-GFP for 24 h were subsequently infected with *bcssp2-12* or B05.10 strains for 24 h, and the edge area of the infected leaves was subjected for confocal imaging and relative fluorescent intensity analysis.

RNA seq analysis

For transcriptome analysis of *B. cinerea* genes during infection, total RNAs were extracted from *Arabidopsis* (Col-0) leaves after inoculation with *B. cinerea* for 24 h, or from *B. cinerea* hypha grown on PDA medium (control group). Qualified RNAs were sent to BGI for RNA-seq by BGISEQ-500 platform. The clean reads were mapped to *B. cinerea* genome using HISAT2 and differently expressed genes were filtered out by DESeq2. The cut-offs for fold-change and FDR were set at 2 and 0.05, respectively. The whole sequencing data were deposited in the NCBI database (GSE217021; token: cpcdiukqfrydrct).

Phylogenetic analysis of BcSSP2

For constructing the phylogenetic tree for BcSSP2, the protein sequence of BcSSP2 (XP_001559885.1) was blasted against the NCBI Reference protein database via BlastP. Among the 85 protein sequences that showed significant alignments (E-value < 0.05) with BcSSP2, the best-aligned sequences from each species were selected for the phylogenetic tree construction. The phylogenetic tree was constructed by MEGA-X using the maximum likelihood method (Whelan and Goldman model) with the default parameters.

Statistics and reproducibility

No statistical method was used to predetermine sample size. No data were excluded from the analyses. The experiments were not randomized. The Investigators were not blinded to allocation during experiments and outcome assessment.

Reporting summary

Further information on research design is available in the Nature Portfolio Reporting Summary linked to this article.

Data availability

The RNA-seq data generated in this study have been deposited in the NCBI GEO under accession numbers GSE217021. The processed RNA-seq data are available at Supplementary Data. All other data supporting the findings of this study are available in the main text, Supplementary Information or Source Data files. Source data are provided with this paper.

References

1. Jones, J. D., Vance, R. E. & Dangl, J. L. Intracellular innate immune surveillance devices in plants and animals. *Science* **354**, aaf6395 (2016).
2. Guo, Z., Li, Y. & Ding, S. W. Small RNA-based antimicrobial immunity. *Nat. Rev. Immunol.* **19**, 31–44 (2019).
3. Jones, J. D. & Dangl, J. L. The plant immune system. *Nature* **444**, 323–329 (2006).
4. Leary, A. Y., Savage, Z., Tumtas, Y. & Bozkurt, T. O. Contrasting and emerging roles of autophagy in plant immunity. *Curr. Opin. Plant Biol.* **52**, 46–53 (2019).
5. Banani, S. F., Lee, H. O., Hyman, A. A. & Rosen, M. K. Biomolecular condensates: organizers of cellular biochemistry. *Nat. Rev. Mol. Cell Biol.* **18**, 285–298 (2017).
6. Jain, S. et al. ATPase-modulated stress granules contain a diverse proteome and substructure. *Cell* **164**, 487–498 (2016).
7. Protter, D. S. W. & Parker, R. Principles and properties of stress granules. *Trends Cell Biol.* **26**, 668–679 (2016).
8. Du, M. & Chen, Z. J. DNA-induced liquid phase condensation of cGAS activates innate immune signaling. *Science* **361**, 704–709 (2018).
9. Slavik, K. M. et al. cGAS-like receptors sense RNA and control 3′2′-cGAMP signaling in Drosophila. *Nature* **597**, 109–113 (2021).
10. Xu, G. et al. Viral tegument proteins restrict cGAS-DNA phase separation to mediate immune evasion. *Mol. Cell* **81**, 2823–2837 e2829 (2021).
11. Mathieu, C., Pappu, R. V. & Taylor, J. P. Beyond aggregation: Pathological phase transitions in neurodegenerative disease. *Science* **370**, 56–60 (2020).
12. Wang, J. et al. Phase separation of nuclear pore complex facilitates selective nuclear transport to regulate plant defense against pathogen and pest invasion. *Mol. Plant* **16**, 1016–1030 (2023).
13. Huang, S., Zhu, S., Kumar, P. & MacMicking, J. D. A phase-separated nuclear GBPL circuit controls immunity in plants. *Nature* **594**, 424–429 (2021).
14. Zavaliev, R., Mohan, R., Chen, T. & Dong, X. Formation of NPR1 condensates promotes cell survival during the plant immune response. *Cell* **182**, 1093–1108 e1018 (2020).
15. Zhou, Y. et al. Plant HEM1 specifies a condensation domain to control immune gene translation. *Nat. Plants* **9**, 289–301 (2023).
16. Song, W. et al. Substrate-induced condensation activates plant TIR domain proteins. *Nature* **627**, 847–853 (2024).
17. Lo Presti, L. et al. Fungal effectors and plant susceptibility. *Annu. Rev. Plant Biol.* **66**, 513–545 (2015).
18. Wu, Q., Wang, X. & Ding, S. W. Viral suppressors of RNA-based viral immunity: host targets. *Cell Host Microbe* **8**, 12–15 (2010).
19. Xin, X. F. & He, S. Y. *Pseudomonas syringae pv. tomato* DC3000: a model pathogen for probing disease susceptibility and hormone signaling in plants. *Annu Rev. Phytopathol.* **51**, 473–498 (2013).
20. Figueroa, M., Ortiz, D. & Henningsen, E. C. Tactics of host manipulation by intracellular effectors from plant pathogenic fungi. *Curr. Opin. Plant Biol.* **62**, 102054 (2021).
21. Fu, Z. Q. et al. A type III effector ADP-ribosylates RNA-binding proteins and quells plant immunity. *Nature* **447**, 284–288 (2007).
22. Kong, L. et al. A phytophthora effector manipulates host histone acetylation and reprograms defense gene expression to promote infection. *Curr. Biol.* **27**, 981–991 (2017).
23. Ma, Z. et al. A paralogous decoy protects *Phytophthora sojae* apoplastic effector PsXEG1 from a host inhibitor. *Science* **355**, 710–714 (2017).
24. Wu, D. et al. Viral effector protein manipulates host hormone signaling to attract insect vectors. *Cell Res.* **27**, 402–415 (2017).
25. Jelenska, J., van Hal, J. A. & Greenberg, J. T. *Pseudomonas syringae* hijacks plant stress chaperone machinery for virulence. *Proc. Natl Acad. Sci. USA* **107**, 13177–13182 (2010).
26. Duan, C. G. et al. Suppression of *Arabidopsis* ARGONAUTE1-mediated slicing, transgene-induced RNA silencing, and DNA methylation by distinct domains of the *Cucumber mosaic virus* 2b protein. *Plant Cell* **24**, 259–274 (2012).
27. Dean, R. et al. The Top 10 fungal pathogens in molecular plant pathology. *Mol. Plant Pathol.* **13**, 414–430 (2012).
28. Williamson, B., Tudzynski, B., Tudzynski, P. & van Kan, J. A. *Botrytis cinerea*: the cause of grey mould disease. *Mol. Plant Pathol.* **8**, 561–580 (2007).
29. Heard, S., Brown, N. A. & Hammond-Kosack, K. An interspecies comparative analysis of the predicted secretomes of the necrotrophic plant pathogens *Sclerotinia sclerotiorum* and *Botrytis cinerea*. *PLoS One* **10**, e0130534 (2015).
30. Veloso, J. & van Kan, J. A. L. Many shades of grey in Botrytis-host plant interactions. *Trends Plant Sci.* **23**, 613–622 (2018).
31. Weiberg, A. et al. Fungal small RNAs suppress plant immunity by hijacking host RNA interference pathways. *Science* **342**, 118–123 (2013).
32. Zhu, W. et al. *Botrytis cinerea* BcSSP2 protein is a late infection phase, cytotoxic effector. *Environ. Microbiol.* **24**, 3420–3435 (2022).
33. Denton-Giles, M. et al. Conservation and expansion of a necrosis-inducing small secreted protein family from host-variable phytopathogens of the Sclerotiniaceae. *Mol. Plant Pathol.* **21**, 512–526 (2020).
34. Petersen, T. N., Brunak, S., von Heijne, G. & Nielsen, H. SignalP 4.0: discriminating signal peptides from transmembrane regions. *Nat. Methods* **8**, 785–786 (2011).
35. Henry, E., Toruno, T. Y., Jauneau, A., Deslandes, L. & Coaker, G. Direct and indirect visualization of bacterial effector delivery into diverse plant cell types during infection. *Plant Cell* **29**, 1555–1570 (2017).
36. Frey, S. et al. Surface properties determining passage rates of proteins through nuclear pores. *Cell* **174**, 202–217 e209 (2018).
37. Li, J. et al. Plant PR1 rescues condensation of the plastid iron-sulfur protein by a fungal effector. *Nat. Plants* **10**, 1775–1789 (2024).
38. Li, X. & Gu, Y. Structural and functional insight into the nuclear pore complex and nuclear transport receptors in plant stress signaling. *Curr. Opin. Plant Biol.* **58**, 60–68 (2020).
39. Lin, D. H. & Hoelz, A. The structure of the nuclear pore complex. *Annu. Rev. Biochem.* **88**, 725–783 (2019).
40. Beck, M. & Hurt, E. The nuclear pore complex: understanding its function through structural insight. *Nat. Rev. Mol. Cell Biol.* **18**, 73–89 (2017).
41. Boeglin, M. et al. Reduced expression of *AtNUP62* nucleoporin gene affects auxin response in *Arabidopsis*. *BMC Plant Biol.* **16**, 2 (2016).
42. Cheng, Y. T. et al. Nuclear pore complex component MOS7/Nup88 is required for innate immunity and nuclear accumulation of defense regulators in *Arabidopsis*. *Plant Cell* **21**, 2503–2516 (2009).
43. Gu, Y. et al. Nuclear pore permeabilization is a convergent signaling event in effector-triggered immunity. *Cell* **166**, 1526–1538 e1511 (2016).
44. Zhang, Y. & Li, X. A putative nucleoporin 96 Is required for both basal defense and constitutive resistance responses mediated by *suppressor of npr1-1, constitutive 1*. *Plant Cell* **17**, 1306–1316 (2005).
45. Schumacher, J., Studt, L. & Tudzynski, P. The putative H3K36 demethylase BcKDM1 affects virulence, stress responses and photomorphogenesis in Botrytis cinerea. *Fungal Genet Biol.* **123**, 14–24 (2019).
46. An, B. et al. Aquaporin8 regulates cellular development and reactive oxygen species production, a critical component of virulence in Botrytis cinerea. *N. Phytologist* **209**, 1668–1680 (2016).
47. Oh, S.-K. et al. In Planta expression screens of *Phytophthora infestans* RXLR effectors reveal diverse phenotypes, including activation

of the *Solanum bulbocastanum* disease resistance protein Rpi-blb2. *Plant Cell* **21**, 2928–2947 (2009).
48. Fang, A. et al. Identification and characterization of plant cell death-inducing secreted proteins from *Ustilaginoidea virens*. *Mol. Plant Microbe Interact.* **29**, 405–416 (2016).
49. Kale, S. D. et al. External lipid PI3P mediates entry of eukaryotic pathogen effectors into plant and animal host cells. *Cell* **142**, 284–295 (2010).
50. Fang, X. et al. Arabidopsis FLL2 promotes liquid-liquid phase separation of polyadenylation complexes. *Nature* **569**, 265–269 (2019).
51. Lin, Y., Protter, D. S., Rosen, M. K. & Parker, R. Formation and maturation of phase-separated liquid droplets by RNA-binding proteins. *Mol. Cell* **60**, 208–219 (2015).
52. Frey, S. & Gorlich, D. A saturated FG-repeat hydrogel can reproduce the permeability properties of nuclear pore complexes. *Cell* **130**, 512–523 (2007).
53. Kong, F., Garcia, A. J., Mould, A. P., Humphries, M. J. & Zhu, C. Demonstration of catch bonds between an integrin and its ligand. *J. Cell Biol.* **185**, 1275–1284 (2009).

Acknowledgements

We thank Paul Tudzynski (University of Münster, Germany) for providing *B. cinerea* stains; Chang He and Xiaokang Zhang (Institute of Botany, the Chinese Academy of Sciences) for help with *B. cinerea* transformation; Jizhong Lou, Hui Chen and Yanruo Zhang (Institute of Biophysics, Chinese Academy of Sciences) for help with AFM experiments; Huizhen Cao and Jinyu Wang (Center of Biomedical Analysis, Tsinghua University) for help with confocal imaging. This research was supported by funding from the National Natural Science Foundation of China (Grant no. 32250001 and Grant no. 32388101 to D.X., Grant no. 32125010 and 32330024 to P.L., Grant no. 32402306 to J.W., Grant no. 32400560 to G.P.); the National Key Research and Development Program of China (2022YFD1400800 and 2021YFA1300400 to D.X., 2023YFF1204703 to P.L.); the Beijing Natural Science Foundation (Grant no. Z230014 to P.L.); the Postdoctoral Fellowship Program of CPSF (Grant no. GZC20240859 to G.P.); the Shuimu Tsinghua Scholar Program (Grant no. 2023SM250 to G.P.); the Postdoctoral Fellowship of the Tsinghua-Peking University Joint Center for Life Sciences (G.P.); the Advanced Innovation Fellow Program (G.P.).

Author contributions

D.X., X.S. and P.L. conceived the study; D.X., J.W. designed the experiments; J.W., D.W., G.P., and Y.W. performed most of the experiments with assistance from X.L., S.T., Z.Z. and X.Z.; J.W. and D.W. wrote the manuscript; D.X., P.L., X.S., J.W., D.W., G.P., and Y.W. revised the paper.

Competing interests

The authors declare no competing interests.

Additional information

Supplementary information The online version contains supplementary material available at https://doi.org/10.1038/s41467-025-63632-7.

Correspondence and requests for materials should be addressed to Jiaojiao Wang, Pilong Li, Daoxin Xie or Xiaoyi Shan.

Peer review information *Nature Communications* thanks Matthias Hahn, Shuai Huang and the other anonymous reviewer(s) for their contribution to the peer review of this work. A peer review file is available.